

Electronic Supporting Information (ESI) for:

**Long-Range Magnetic Order in the Porous Metal-Organic Framework
Ni(pyrazine)[Pt(CN)₄]**

J. Alberto Rodríguez-Velamazán,^{*[a]} Olivier Roubeau,^[b] Roberta Poloni,^[c] Elsa Lhotel,^[d] Elías Palacios,^[b] M. González,^[a] José A. Real^[e]

[a] Institut Laue-Langevin, F-38042 Grenoble, France

[b] Instituto de Ciencia de Materiales de Aragón (ICMA), CSIC and Universidad de Zaragoza, E-50009, Zaragoza, Spain

[c] SIMAP, CNRS and Université Grenoble Alpes, F-38000 Grenoble, France

[d] Institut Néel, CNRS and Université Grenoble Alpes, F-38042 Grenoble, France

[e] Instituto de Ciencia Molecular (ICMol), Universidad de Valencia, Paterna, E-46980 Valencia, Spain

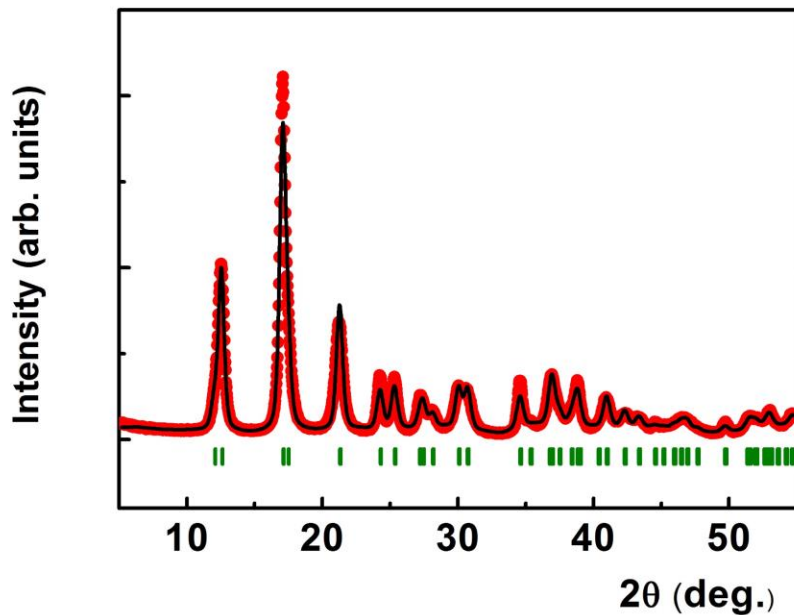


Figure S1. X-ray diffraction pattern of $\{\text{Ni}(\text{pyrazine})[\text{Pt}(\text{CN})_4]\}$ recorded at room temperature using $\text{Cu K}\alpha$ radiation. Experimental pattern (red symbols), profile fit (black line) and Bragg peak positions (green marks). The diffractogram well corresponds to the structure of the isostructural compounds ($P4/mmm$ space group), with no sign of impurities.

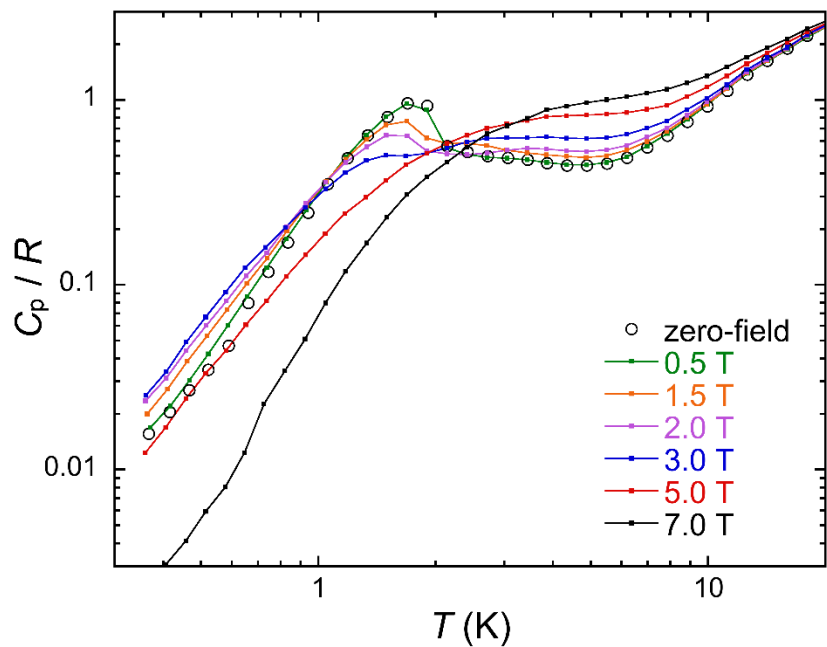


Figure S2. Molar heat capacity of $\{\text{Ni}(\text{pyrazine})[\text{Pt}(\text{CN})_4]\}$ normalized to the gas constant R in zero-field (empty circles) and at different applied magnetic fields (lines+dots).

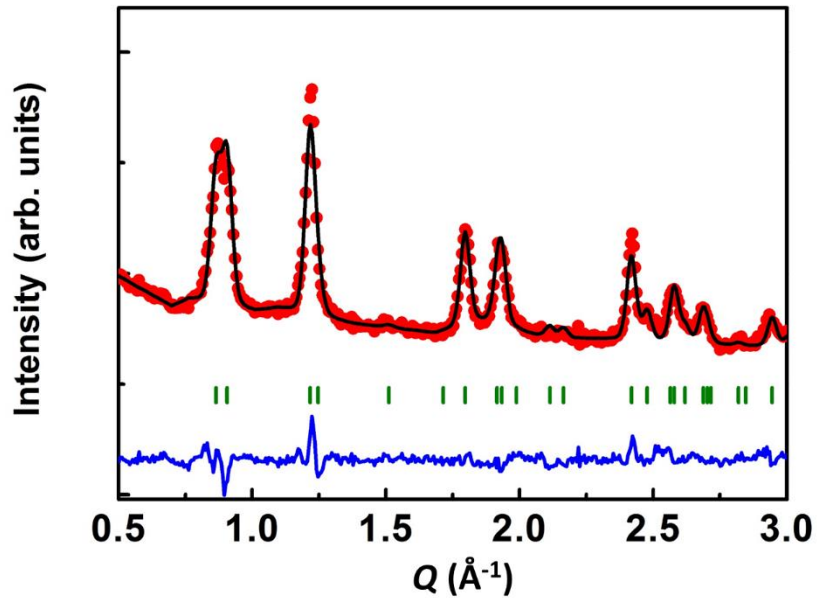


Figure S3. Neutron diffraction pattern of $\{\text{Ni}(\text{pyrazine})[\text{Pt}(\text{CN})_4]\}$ at 5 K (red symbols), Rietveld fit (black line), difference (blue line) and Bragg peak positions (green marks). The fit was done starting from the structure of the isostructural compounds, with $P4/mmm$ space group and refined cell parameters $a = 7.38(1)$ Å and $c = 7.05(1)$ Å. No further refinement of the structure was carried out due to the limitations of the data quality.

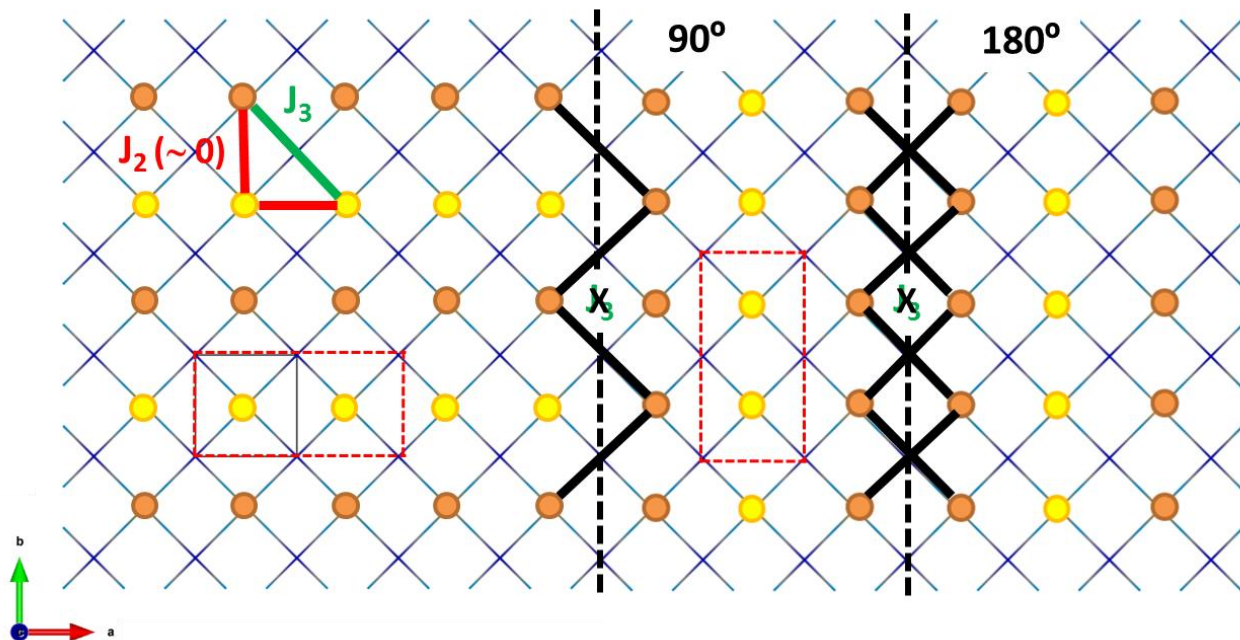


Figure S4. Scheme of the spin arrangement resulting from an antiferromagnetic next-nearest-neighbour interaction through the metallo-cyanide ligands (J_3) and a nearly null nearest-neighbour magnetic interaction (J_2). Orange and yellow points indicate magnetic moments oriented positive and negative, respectively. Black dashed lines separate regions with different equivalent configurations, while black continuous lines indicate infringements of the J_3 antiferromagnetic interaction in the borders. The grey continuous line stands for the crystal unit cell, while the red dashed line represent the magnetic unit cell, corresponding to a magnetic propagation vector $\mathbf{k} = [\frac{1}{2}, 0, \frac{1}{2}]$ (left) or equivalently $\mathbf{k} = [0, \frac{1}{2}, \frac{1}{2}]$ (center and right).

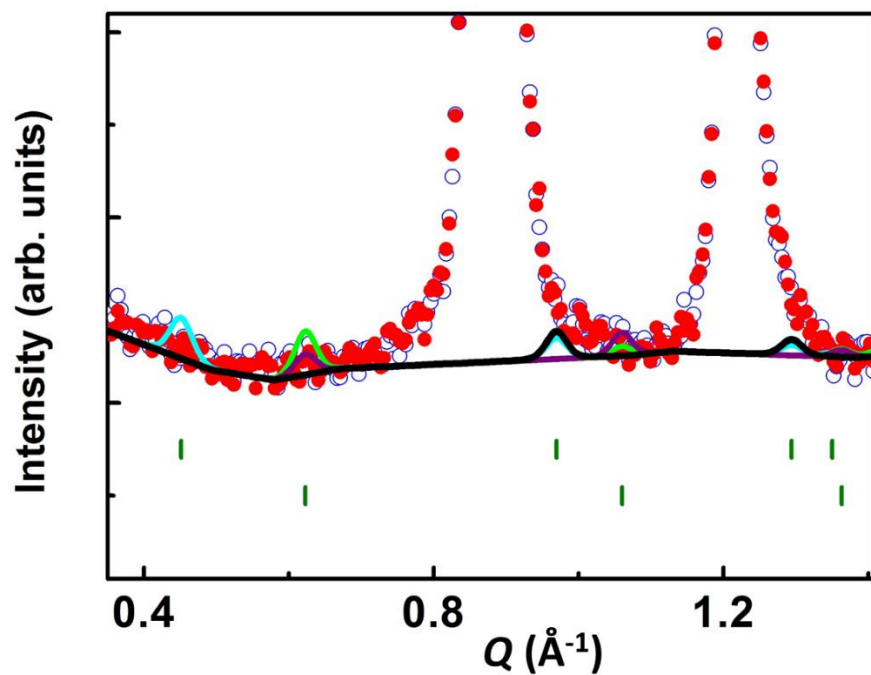


Figure S5. Neutron diffraction data in the low Q region and comparison with the calculation of the magnetic contribution (summed to the background) for four possible magnetic structures: with $\mathbf{k} = [0, 0, \frac{1}{2}]$ and the moments along c (black line) and in the ab plane (cyan line), and with $\mathbf{k} = [\frac{1}{2}, 0, \frac{1}{2}]$ and the moments along c (purple line) and in the ab plane (light green line) The vertical bars mark the positions of the magnetic reflections.

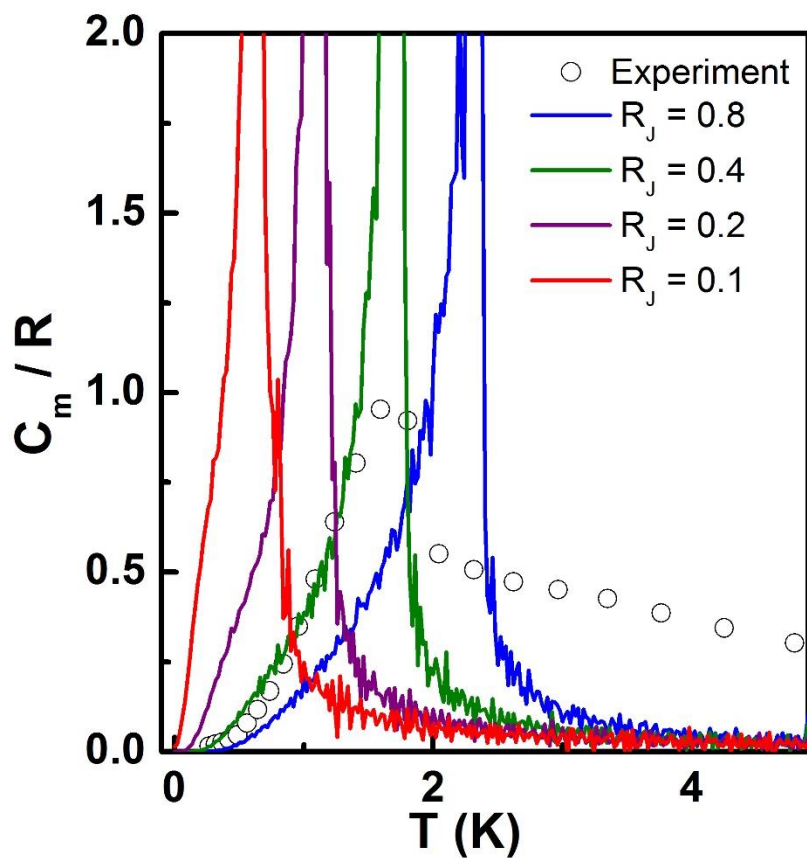


Figure S6. Experimental magnetic heat capacity of $\{\text{Ni}(\text{pyrazine})[\text{Pt}(\text{CN})_4]\}$ normalized to the gas constant R in zero-field (empty circles) compared with the results of Monte Carlo (MC) simulations with total energy 3.3 K and different values of the ratio $R_J = J_3/J_1$ (lines). The Monte Carlo simulations have been performed with a system of $30 \times 30 \times 30$ spins $S = 1$, using periodic boundary conditions. The simulations follow the standard Metropolis MC algorithm. Starting from a disordered configuration at high temperature, the temperature is lowered in steps $\Delta T = 0.02$ K. At each temperature, averaging is done over 1000 MC sweeps, after having discarded previously 500 MC sweeps to let the system equilibrate. We obtain the heat capacity as the derivative of the magnetic energy.